1985MNRAS.215..773M

Mon. Not. R. astr. Soc. (1985) **215,** 773–797

The morphologies and magnetic field structures of six 3CR double radio galaxies

L. Miller† *Mullard Radio Astronomy Observatory, Cavendish Laboratory, Madingley Road, Cambridge CB3 0HE*

Accepted 1985 March 7. Received 1985 March 7; in original form 1984 January 19

Summary. Observations of the regions of low surface brightness in six 3CR double radio galaxies (3C 98, 184.1, 192, 223, 332 and 430) have been made with the Cambridge 5-km telescope. Maps of total and polarized intensity are presented, and the projected magnetic field structures have been deduced. High fractional polarization is seen in these sources, indicating that the magnetic fields are well-ordered. A qualitative model for the formation of the magnetic field structures is presented, in which pressure gradients in the extended lobes cause bulk flow of plasma and consequent large-scale shearing of the magnetic fields.

1 Introduction

This paper concerns the radio structures of regions of low surface brightness in six radio galaxies: 3C 98, 184.1, 192, 223, 332 and 430, with redshifts of 0.0306, 0.1182, 0.0599, 0.1368, 0.1515, and 0.0541 respectively (Smith & Spinrad 1980). They are known to have double radio structures of Fanaroff & Riley's (1974) class II from earlier 5-GHz maps (Jenkins, Pooley & Riley 1977; Riley & Pooley 1975; Högbom 1979), but 5-GHz polarization maps were made only of 3C 192 and 223 (Högbom 1979). In addition, Burch (1979a) mapped 3C 430 at 2.7 GHz in total power and polarization and more recently Spangler, Myers & Pogge (1984) have mapped this source at 1446 and 4885 MHz. The present observations comprise maps in total power and polarization of all but 3C 430 at 2.7 GHz, and of 3C 192 and 430 at 5 GHz.

When observed at arcsec resolution, the extended structures in class II sources frequently show a high degree of polarization, and the projected field directions are correlated with the source structure (e.g. Laing 1981a). The high degree of polarization shows that, when projected onto the plane of the sky, the field structure must be well-ordered on the scale of the telescope resolution. The correlations with source structure indicate that the ordered components are produced by dynamical effects in the source. Theoretical considerations have suggested how this might arise (Blandford & Rees 1974, 1978), and Laing (1980, 1981b) has described an empirical model which is in general agreement with the observations. In this paper the field structures will be investigated in more detail, and consideration is given to the dynamical effects on the field structures of pressure gradients with the sources.

†Present address: Department of Astronomy, University of Edinburgh, Blackford Hill, Edinburgh EH9 3HJ, Scotland.

© Royal Astronomical Society • Provided by the NASA Astrophysics Data System

1985MNRAS.215..773M

2 Observations and results

These observations were made with the Cambridge 5-km telescope (Ryle 1972)at frequencies of 2.695 and 4.995 GHz. A Gaussian weighting of the aperture to 30 per cent at the maximum baseline of 4.57 km was adopted, resulting in half-power beamwidths of 3.7×3.7 cosec δ arcsec^2 at 2.7 GHz and of 2×2 cosec δ arcsec^2 at 5 GHz. Generally, sufficient observations were made of the Stokes' parameters I–Q, Q, and U for each source to ensure adequate oversampling, as described by Jenkins *et al.* (1977). 3C 184.1, 192 and 223, at 2.7 GHz, and 3C 430 at 5 GHz were each observed for four 12-hr periods both in I–Q, and in Q and U. 3C 98 was observed for four 12-hr periods in I–Q and two 12-hr periods in the polarization mode, 3C 332 for one 12-hr period in each mode, and 3C 192 for eight 12-hr periods at 5 GHz in each mode. For 3C 98 the source size in right ascension is comparable to the radius of 156 arcsec of the first grating response in the polarization maps. Nevertheless, the grating rings are clear of the source structure and, since we expect the total intensity in Q and U to be low, the polarization zero-level should not be seriously affected. To help offset this problem, the maps of 3C 98 have also been cleaned using standard methods.

Contour maps of Stokes' parameter I are shown in Figs 1–6. A cross marks the position of each optical galaxy, as compiled by Laing, Riley & Longair (1983). Also shown for five sources are the polarization data at 2.7 GHz and maps of the projected magnetic field direction, with vectors whose lengths are proportional to the fractional polarization at each point. The sampling of the polarization data is at intervals of either 1.5×1.5 cosec δ arcsec^2, 2×2 cosec δ arcsec^2 (for 3C 332), or 3×3 cosec δ arcsec^2 (for 3C 98), providing oversampling of 2.5, 1.9 and 1.2 respectively. The rms noise level on the maps of Stokes' parameter I is about 2.6 $n^{1/2}$ mJy for an observation of $n^{1/2}\times12$ hr, and is about 2.1 $n^{1/2}$ mJy on each map of the Stokes' parameters Q and U.

The polarization map of 3C 430 is not included, as this source has a large variation in rotation measure across it, and the magnetic field structure has been discussed by Spangler *et al.* (1984). The map of Stokes' parameter I at 5 GHz is reproduced as this source will also be discussed below. The polarization data for 3C 192 at 5 GHz likewise are not shown, as the signal-to-noise ratio is low at the full resolution.

The projected magnetic field directions for the remaining sources were derived from the polarization observations by means of the integrated rotation measures from Haves (1975) and Conway *et al.* (1983), and the angles through which the **E**-vectors have been rotation to obtain their emitted position angles are given in the figure captions. The variations in position angle with frequency for these sources are fitted well by square-laws, except for a discrepant point at 6 cm for 3C 98. This may indicate the presence of a region of large Faraday depth within this source, but at wavelengths greater than 6 cm the correction for Faraday rotation should be unaffected. No attempt has been made to correct for variations in rotation measure across the sources because, with the exception of 3C 98 which displays moderate rotation, the integrated rotation measures are small (Figs 1–5), so variations in rotation measure should also be small.

Magnetic field data have not been plotted for any region where the total surface brightness was below a threshold given for each map. Unlike the polarization maps, no lower threshold on the polarized intensity has been applied, as the displayed distribution of fractional polarization would then be biased towards high values. The presentation chosen reduces this bias, and although regions with low signal are not reliable indicators of the local fractional polarization and field direction, the larger-scale structures within such regions may still be discerned in many cases. There still remain biases towards high values of fractional polarization due to negative offsets in the I maps, and noise in the maps of polarized intensity. At the threshold levels chosen for I, the former bias is not significant since the zero-level biases are only comparable to the noise levels. The second bias is more critical. In the absence of any signal, the noise in the polarized maps is

© Royal Astronomical Society • Provided by the NASA Astrophysics Data System

1985MNRAS.215..773M

distributed as a Rayleigh distribution with its maximum at 2.1 $n^{-1/2}$ mJy. Thus, as the polarized flux density ot the source approaches this value, the fractional polarization displayed is distributed about a value 2.1 $n^{-1/2}I^{-1}$ for a point on the map with total surface brightness I mJy.

Additional maps with lower resolution, about 10 arcsec, were synthesized for 3C 184.1 and 223, and are also shown in Figs 2 and 4.

3 Notes on the individual sources

Each source will be discussed individually before consideration of the results as a whole.

3C 98. This source (Fig. 1) has prominent lobes, with regions of higher surface brightness extending about 15–20 arcsec from the hotspots. The apparent widths of the lobes decrease close to the galaxy. The projected magnetic field in the southern lobe appears tangential to the boundary, with the fractional polarization rising from low values on the major axis to nearly the maximum values attainable from synchrotron emission (about 70 per cent) around the edges. The field is also tangential to the boundary around part of the northern lobe, although the fractional polarization is lower than in the southern lobe. There is in addition a region with high fractional polarization and a magnetic field transverse to the major axis of the source.

3C 184.1. The source structure (Fig. 2) can be divided into separate regions, namely the hotspots, narrow tails of high surface brightness which extend about 10–15 arcsec back from the hotspots, and broad lobes which occupy the inner 60 per cent of the source and have surface brightnesses fairly constant along the major axis of the source. The magnetic field directions in the regions of high surface brightness are either parallel to the major axis, or follow the boundary of the lobe. Around the edge of the southern inner lobe, the field is also parallel to the boundary, but in the other parts of the inner lobes the field is transverse to the source axis. High fractional polarization, about 30 per cent, is seen in all parts of the lobes, and the fractional polarization does not decrease away from the lobe boundaries. This also appears to be true in the tail region of the southern component, when viewed at higher resolution (Miller & Laing, in preparation).

3C 192. Högbom (1979) has noted the rotational symmetry of this source (Fig. 3). The projected magnetic field is nearly perpendicular to the source axis in the fat, distorted parts of the lobes. Although the field direction is parallel to the distorted boundaries, the field does not appear to follow the contours of surface brightness within these regions. In the narrower outer parts of the lobes the field is parallel to both the source axis and the boundaries of the lobes. High fractional polarizations of about 50 per cent are observed. There are tail regions of high surface brightness close to the hotspots. The high-resolution map (Fig. 3) shows that a large fraction of the north-west hotspot remains unresolved, but that the south-east hotspot and tail are well resolved.

3C 223. This source (Fig. 4) also shows high fractional polarization in the lobes. The field in most of the visible northern and southern lobes is either parallel to the major axis of the source or follows the surface brightness contours, but the lower-resolution maps (Fig. 4d) reveal that the field becomes transverse closer to the galaxy in the northern lobe, as noted by Högbom (1979). The fractional polarization of the tangential components does not decrease away from the edges of the lobe. The lobe appears to decrease in width towards the galaxy, almost certainly due to a decrease in surface brightness arising from spectral steepening (Högbom 1979). A weak hotspot is observed at the extremity of the southern component.

3C 332. There is little polarized signal in this source (Fig. 5), so the magnetic field structure is uncertain, except that the field appears to follow the brightness contours around the southern lobe, and to be transverse in the northern lobe near the central component. There are regions of high surface brightness around the hotspots, and a wide ridge joining the southern hotspot and the central component.

3C 430. This source (Fig. 6) has lobes of high surface brightness which extend completely back

© Royal Astronomical Society • Provided by the NASA Astrophysics Data System

1985MNRAS.215..773M

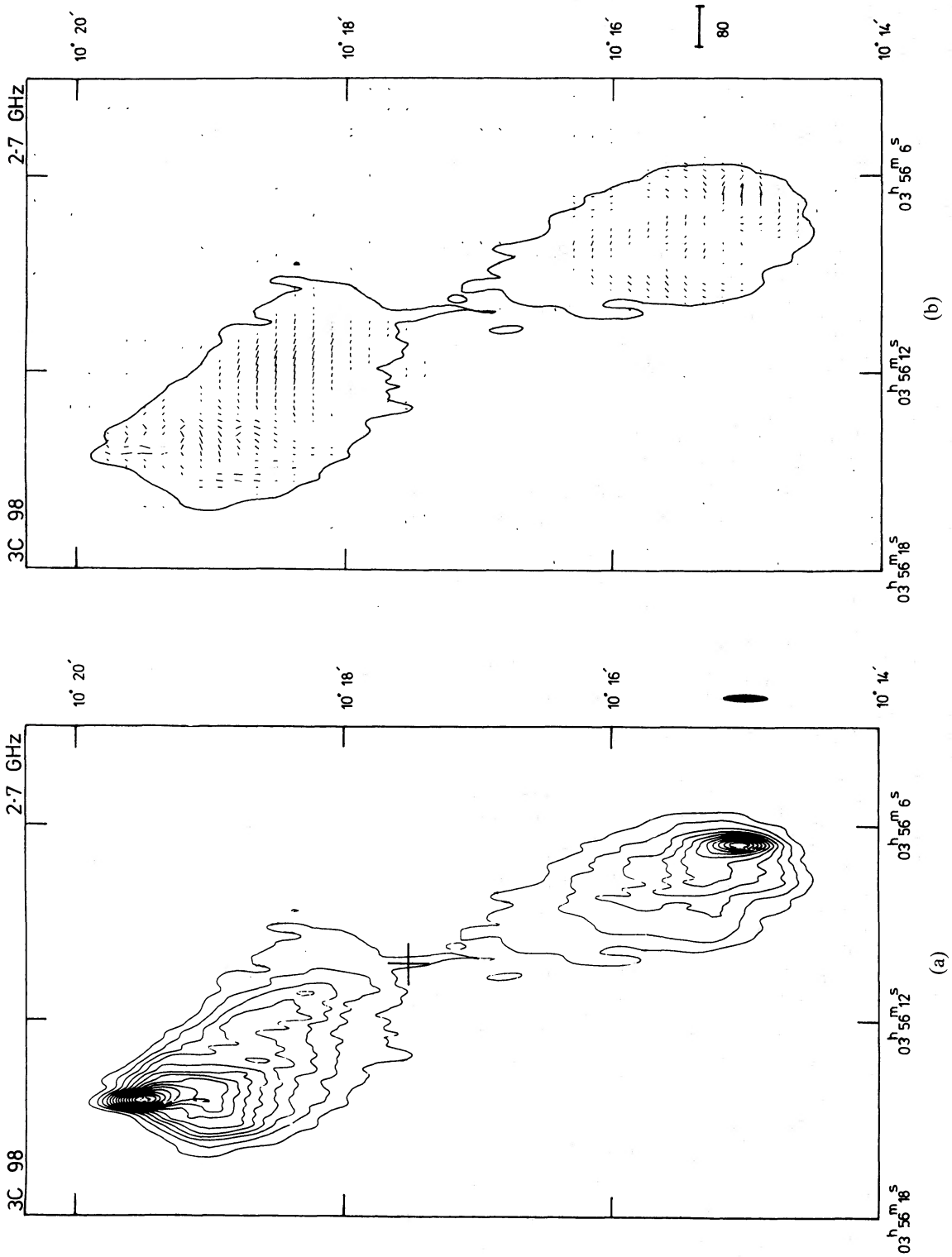

© Royal Astronomical Society • Provided by the NASA Astrophysics Data System

1985MNRAS.215..773M

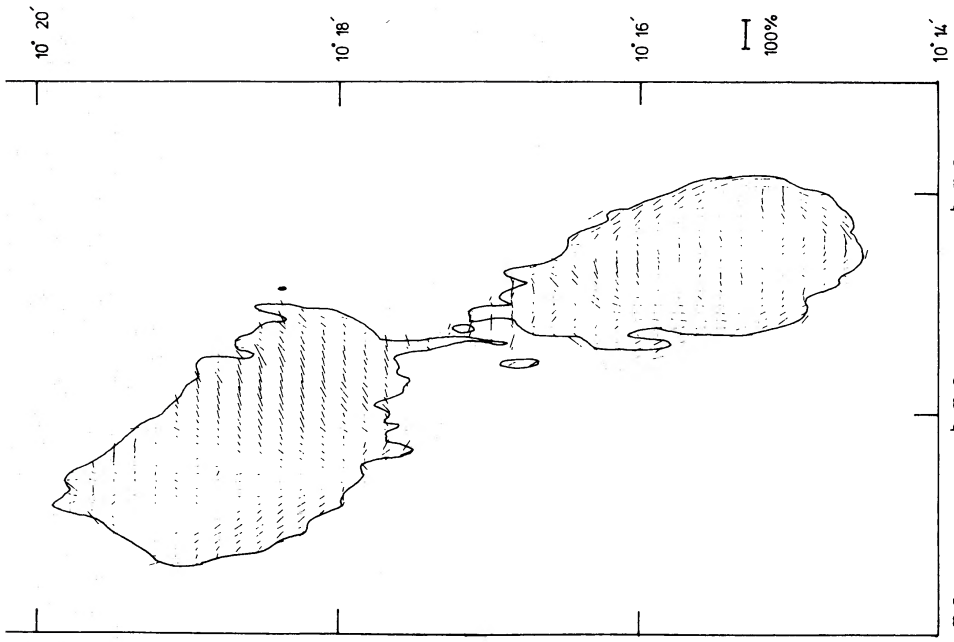

Figure 1. 3C 98 at 2.7 GHz. (a) Map of total intensity, I, with contour levels at intervals of 10 mJy beam^{-1}, starting at 10 mJy beam^{-1}. The scale of brightness temperature, T, is 2.20 K per mJy beam^{-1}. (b) Map of polarized intensity, p, showing the direction of the **E**-field with vector lengths proportional to p. The scale of the vectors is indicated in units of mJy beam^{-1}. Values of p below 4 mJy beam^{-1} are not shown, and the I contour at 10 mJy beam^{-1} is drawn. (c) Map of projected magnetic field direction. Vector lengths are proportional to fractional polarization, and are not shown where I<10 mJy beam^{-1}. The correction for Faraday rotation is −54°.

© Royal Astronomical Society • Provided by the NASA Astrophysics Data System

1985MNRAS.215..773M

towards the central galaxy,. With a linear size of about 125 kpc, the source is smaller than most of the others discussed here. There is a bright resolved knot about 10 arcsec north of the south-west hotspot, and highly asymmetric emission around the hotspots. The most striking feature of this source is the sideways displacement of the lobe from the major axis. Spangler *et al.* (1984) discuss the projected magnetic field structure and find that it appears circumferential in most of the source, except that it is perpendicular to the source axis on the sharp south-east edge, where there is high fractional polarization.

4 The variation of minimum energy density in the sources

The pressure of radiating relativistic plasma within the sources, and its variation with position, could have important dynamical effects on the field structure. Since the radiating material consists

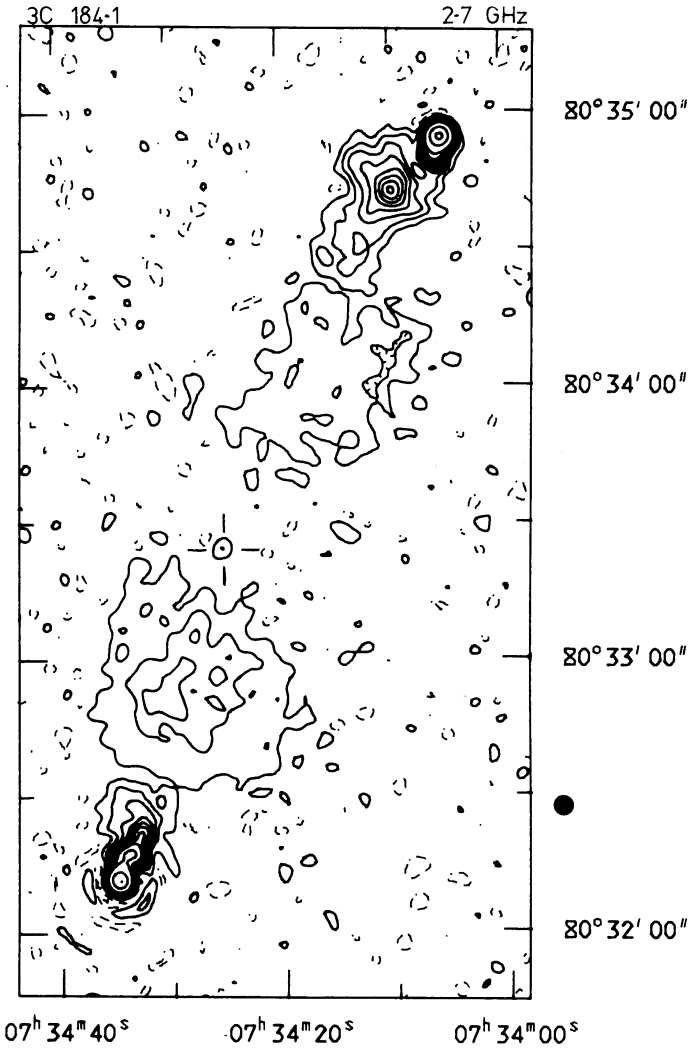

(a)

Figure 2. 3C 184.1 at 2.7 GHz. Captions as for Fig. 1, except as follows: (a) contour levels −2, 2, 6, 10, 14, 18, 22, 26, 30, 40, 80, 120 mJy beam^{-1}, 13.7 K per mJy beam^{-1}; (b) vectors are not shown where $p<2$ mJy beam^{-1}; I contour at 4 mJy beam^{-1}; (c) vectors are not shown where $I<3$ mJy beam^{-1}; the correction for Faraday rotation is 13°; (d) maps convolved to about 10 arcsec resolution: (left) total intensity, contours at 20 mJy beam^{-1} interval omitting the zero contour; the scale of T is 2.08 K per mJy beam^{-1}; (centre) polarized intensity where $p>3.5$ mJy beam^{-1}; (right) magnetic field direction where $I>15$ mJy beam^{-1}, with the same rotation correction as (c).

© Royal Astronomical Society • Provided by the NASA Astrophysics Data System

1985MNRAS.215..773M

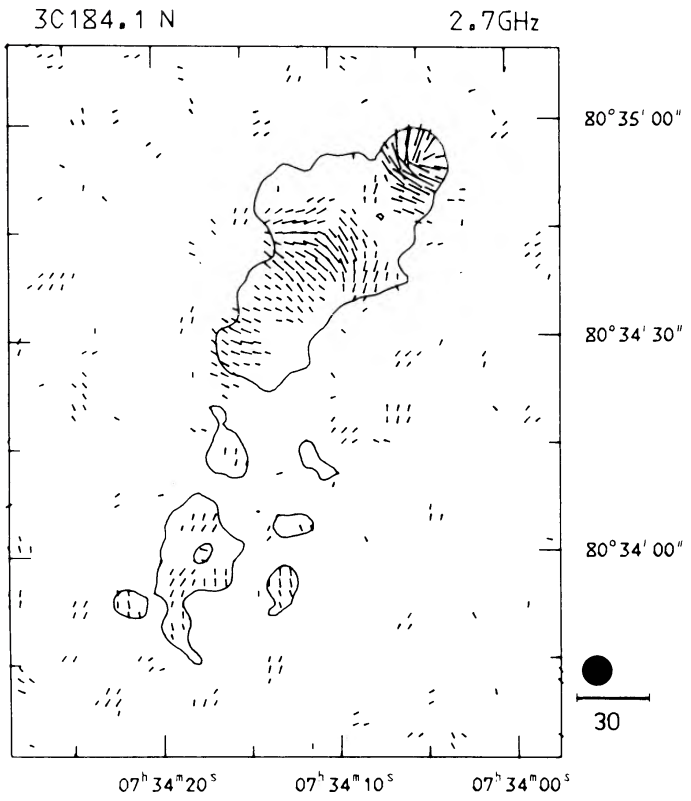

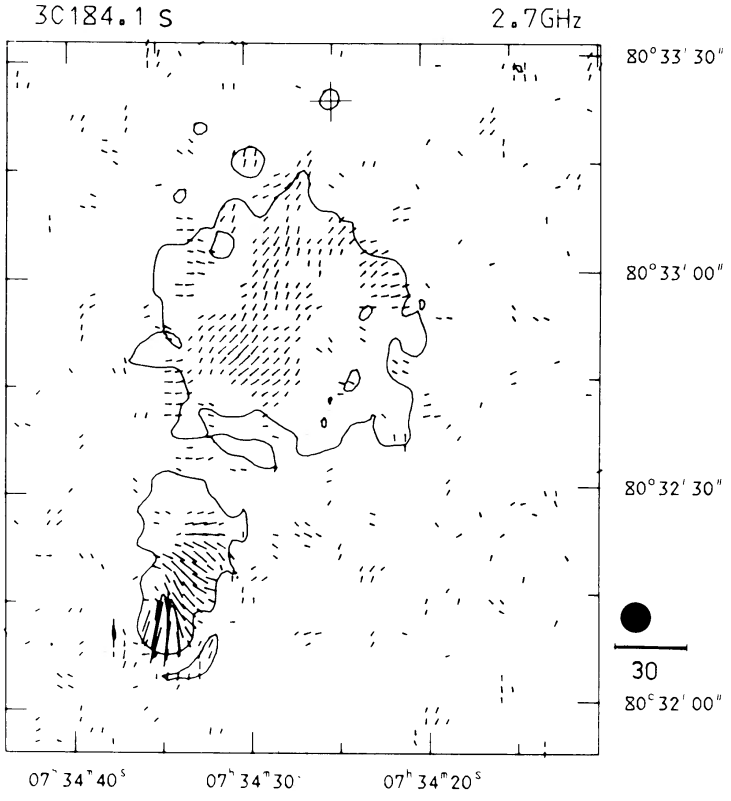

(b)

Figure 2 – *continued*

© Royal Astronomical Society • Provided by the NASA Astrophysics Data System

1985MNRAS.215..773M

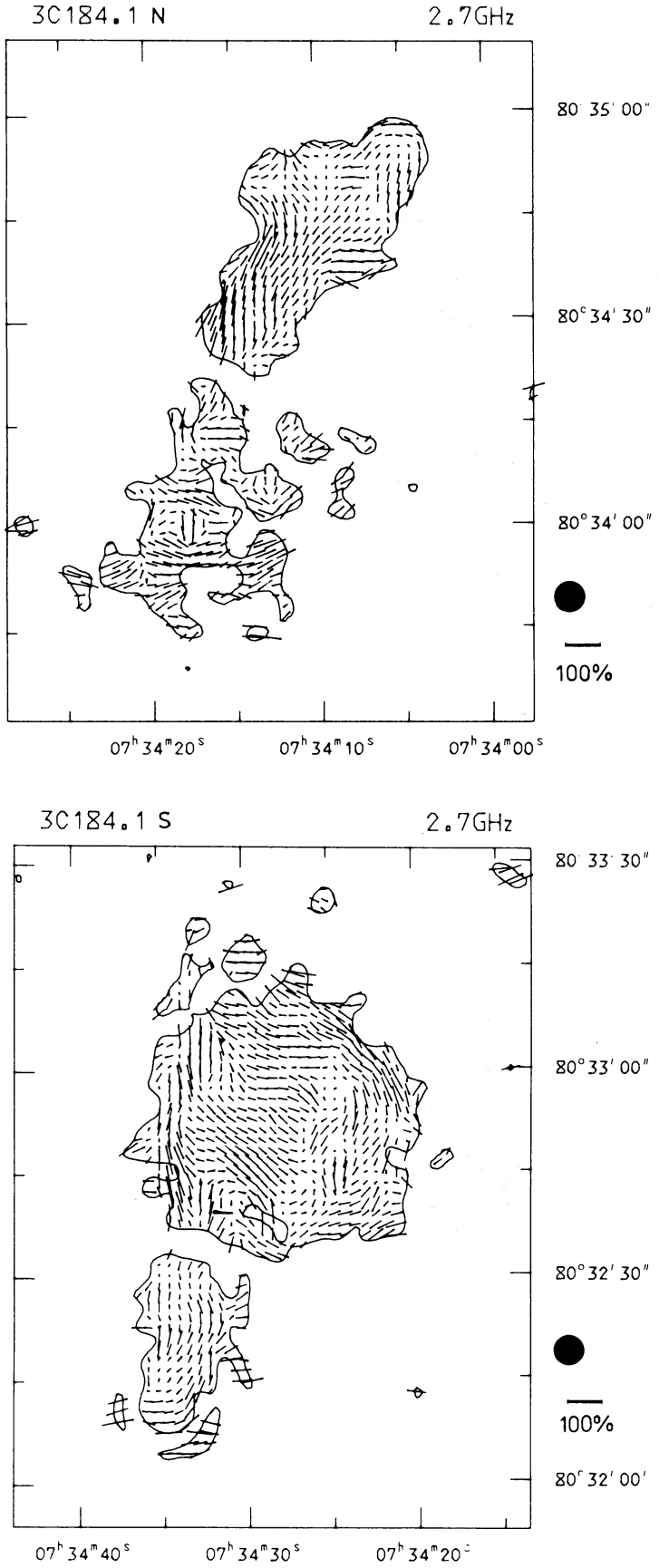

(c)

Figure 2 – *continued*

© Royal Astronomical Society • Provided by the NASA Astrophysics Data System

1985MNRAS.215..773M

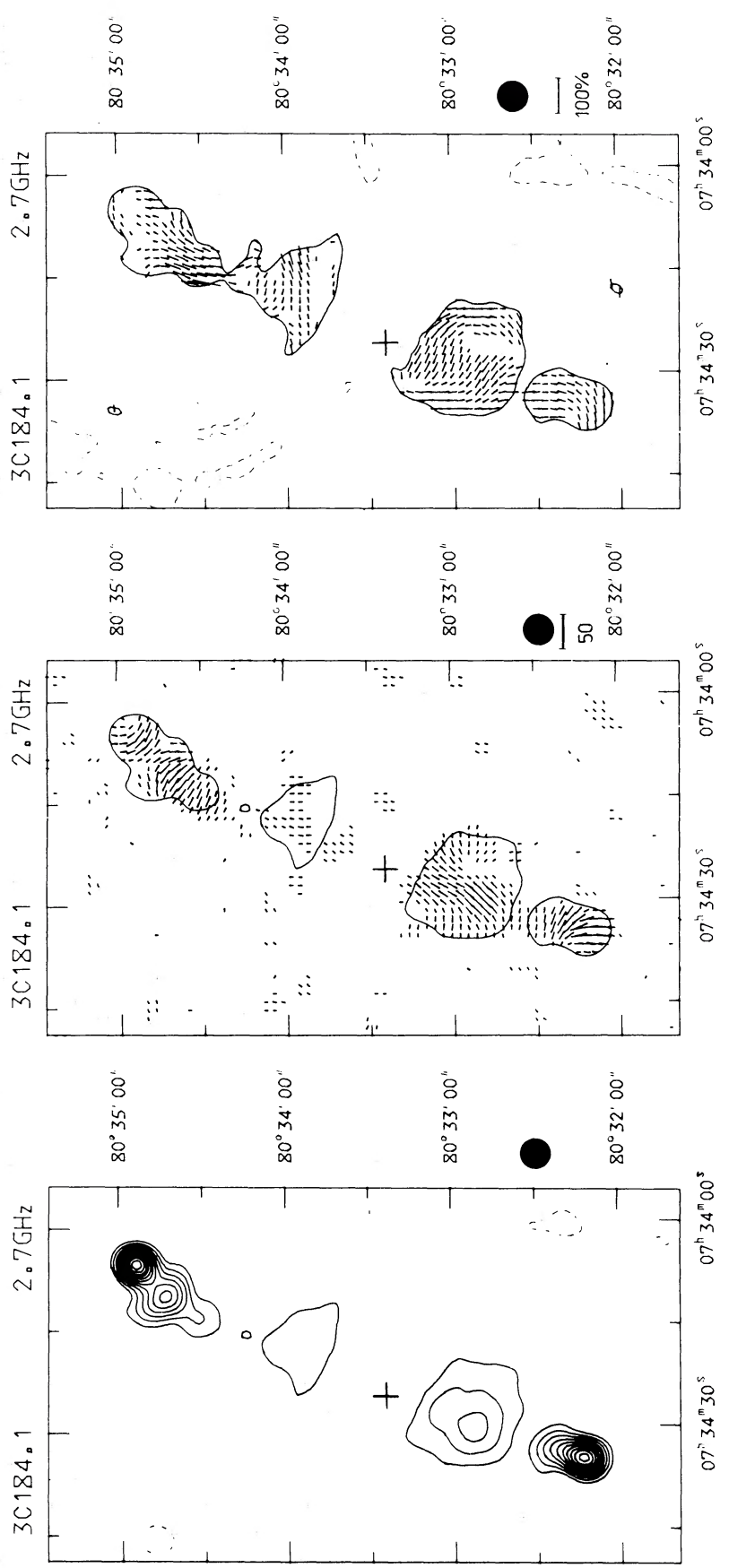

Figure 2 – *continued*.

© Royal Astronomical Society • Provided by the NASA Astrophysics Data System

1985MNRAS.215..773M

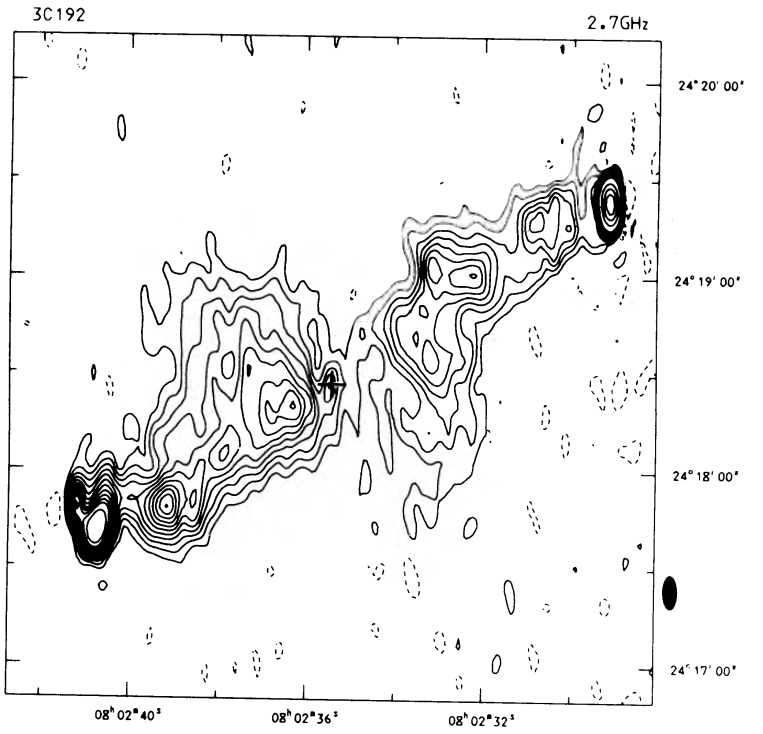

(a)

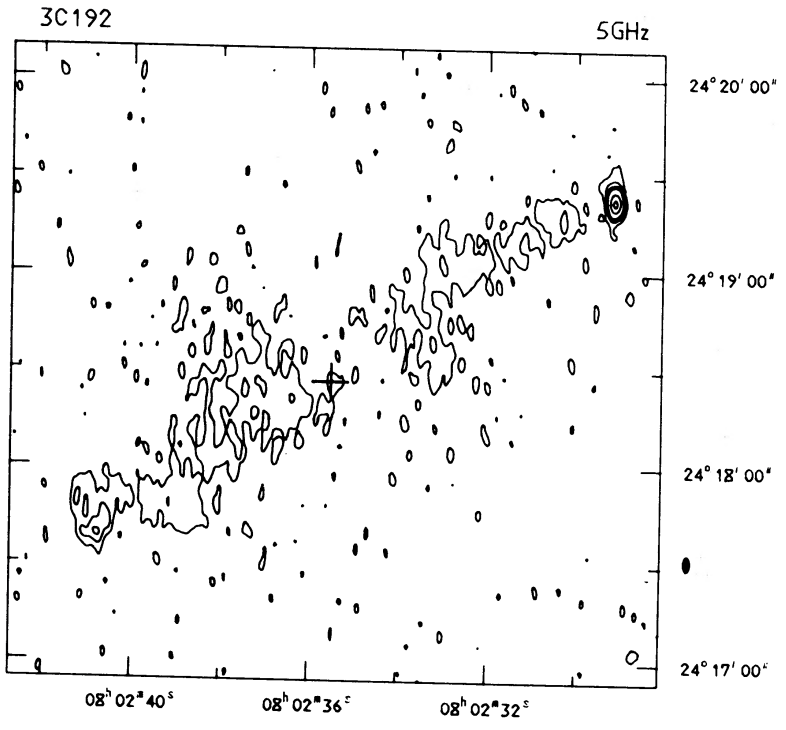

(b)

Figure 3. 3C 192. Captions as for Fig. 1, except as follows: (a) total intensity at 2.7 GHz, with contour levels −3, 3, 6, 9, 12, 15, 18, 21, 24, 27, 30, 33, 40, 80, 120, 160 mJy beam^{-1}, 5.46 K per mJy beam^{-1}; (b) total intensity at 5 GHz; contour levels are −3, 3, 9, 15, 21, 48, 72 mJy beam^{-1}; the scale of T is 5.44 K per mJy beam^{-1}. (c) p at 2.7 GHz; vectors are not shown where p<3 mJy beam^{-1}; I contour at 4 mJy beam^{-1}; (d) projected magnetic field direction; vectors are not shown where I<4 mJy beam^{-1}; the correction for Faraday rotation is −12°.

© Royal Astronomical Society • Provided by the NASA Astrophysics Data System

1985MNRAS.215..773M

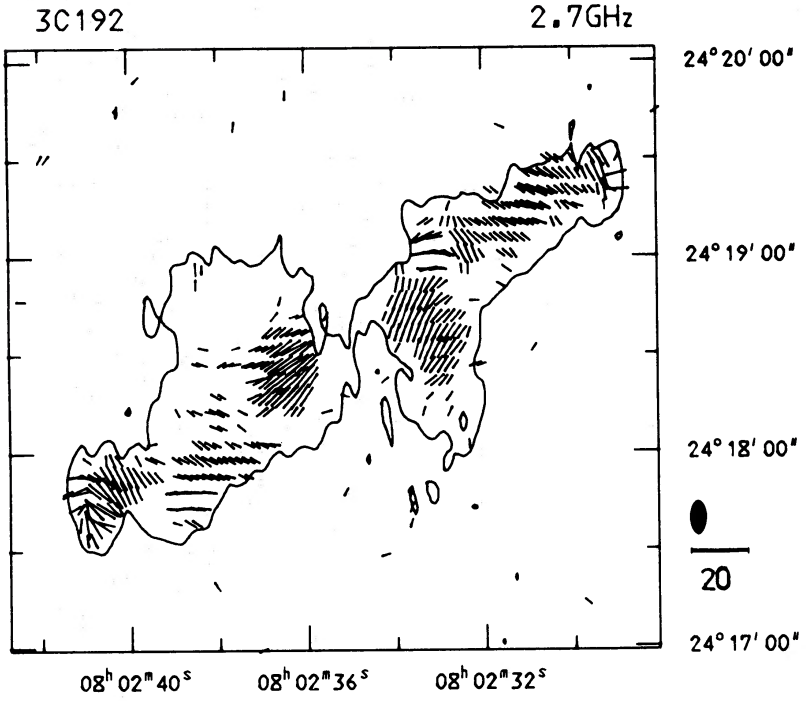

(c)

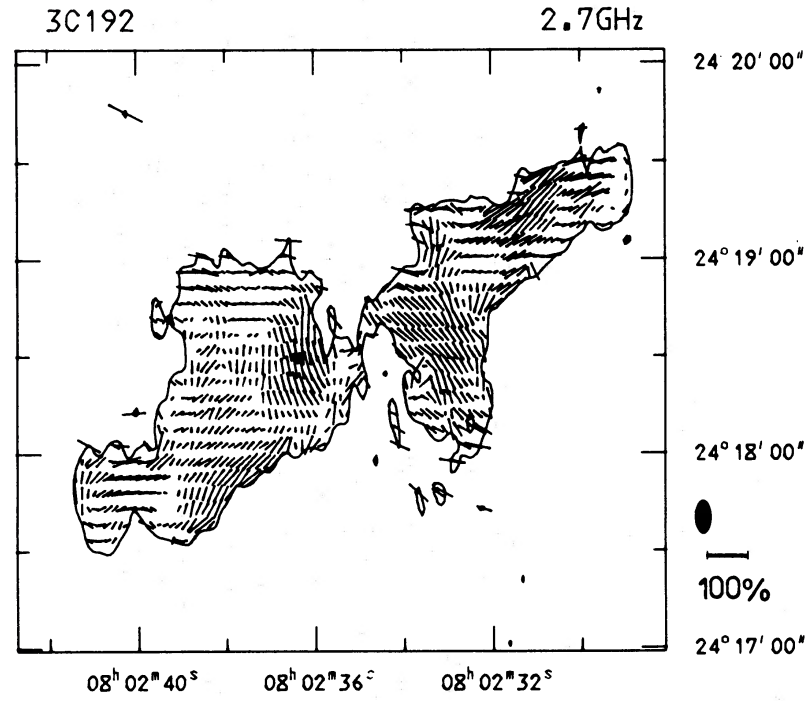

(d)

Figure 3 – *continued*

© Royal Astronomical Society • Provided by the NASA Astrophysics Data System

1985MNRAS.215..773M

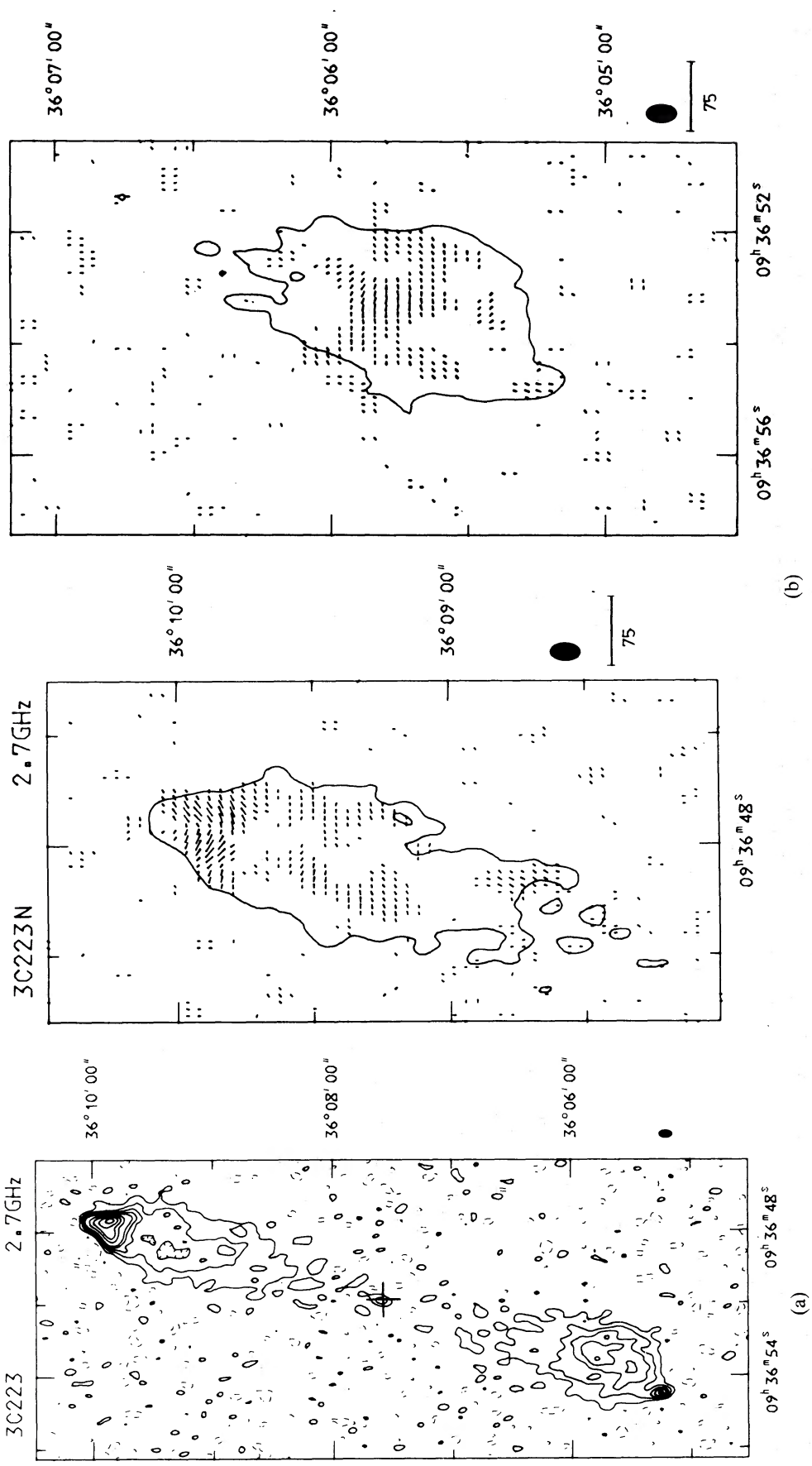

© Royal Astronomical Society • Provided by the NASA Astrophysics Data System

1985MNRAS.215..773M

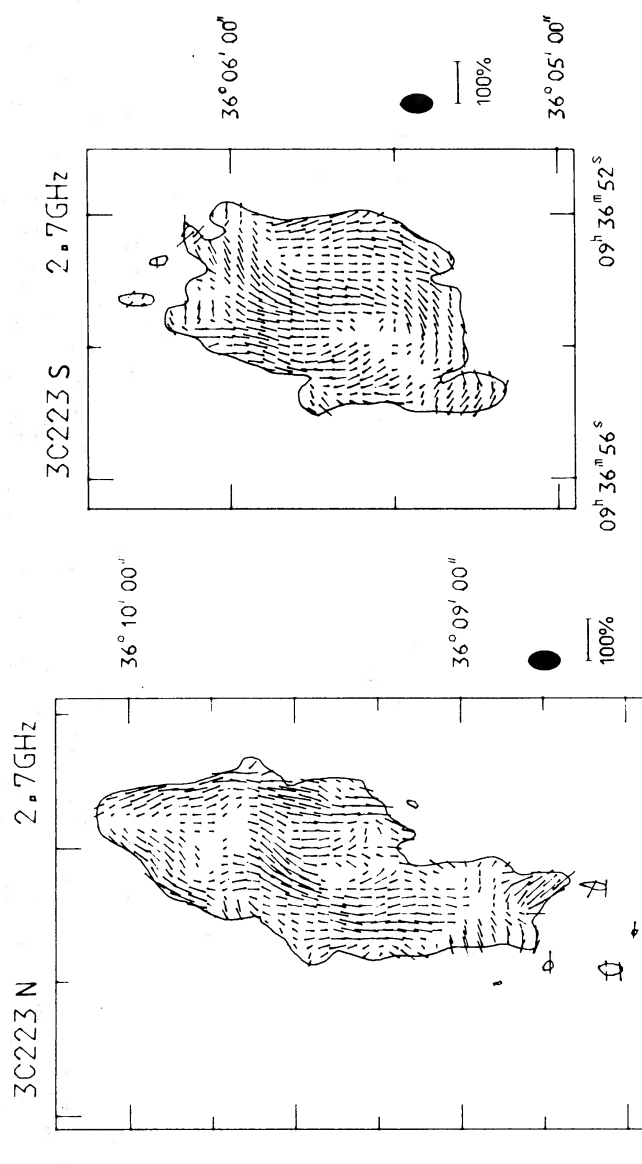

Figure 4. 3C 223 at 2.7 GHz. Captions as for Fig. 1, except as follows: (a) contour levels −2, 2, 6, 10, 14, 18, 30, 40, 50, 60 mJy beam^{-1}, 7.98 K per mJy beam^{-1}; (b) vectors are not shown where $p<2$ mJy beam^{-1}; I contour at 4 mJy beam^{-1}; (c) vectors are not shown where $I<5$ mJy beam^{-1}; the correction for Faraday rotation is −11°; (d) maps convolved to about (10×10 cosec δ) arcsec^2 resolution: (left) total intensity, contours at −7.5, 7.5, 22.5, 37.5, 52.5, 100, 150, 200 mJy beam^{-1}, 1.23 K per mJy beam^{-1}; (centre) polarized intensity where $p>3$ mJy beam^{-1}; (right) magnetic field direction where $I>5$ mJy beam^{-1}, with the same rotation correction as (c).

© Royal Astronomical Society • Provided by the NASA Astrophysics Data System

1985MNRAS.215..773M

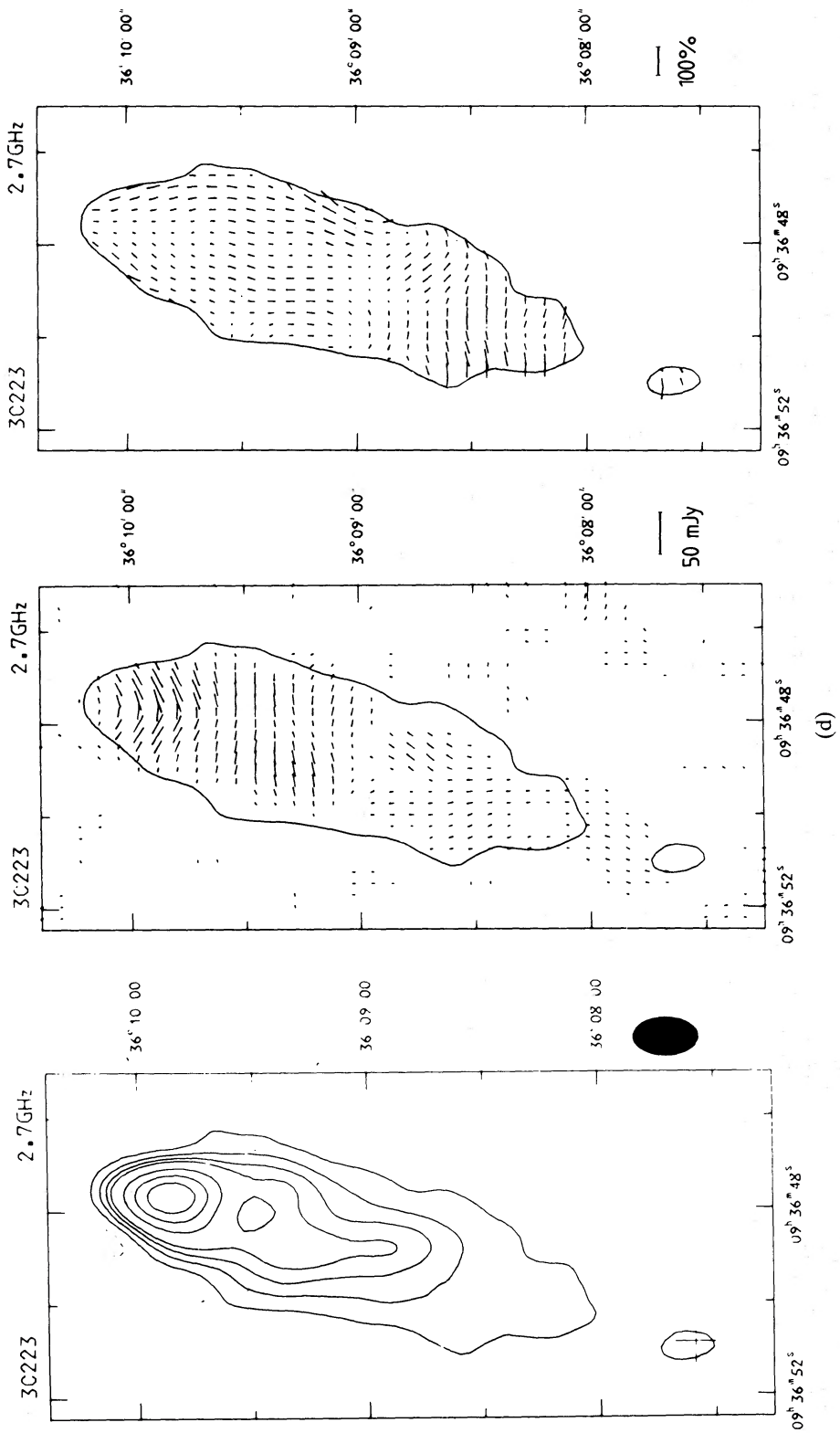

© Royal Astronomical Society • Provided by the NASA Astrophysics Data System

1985MNRAS.215..773M

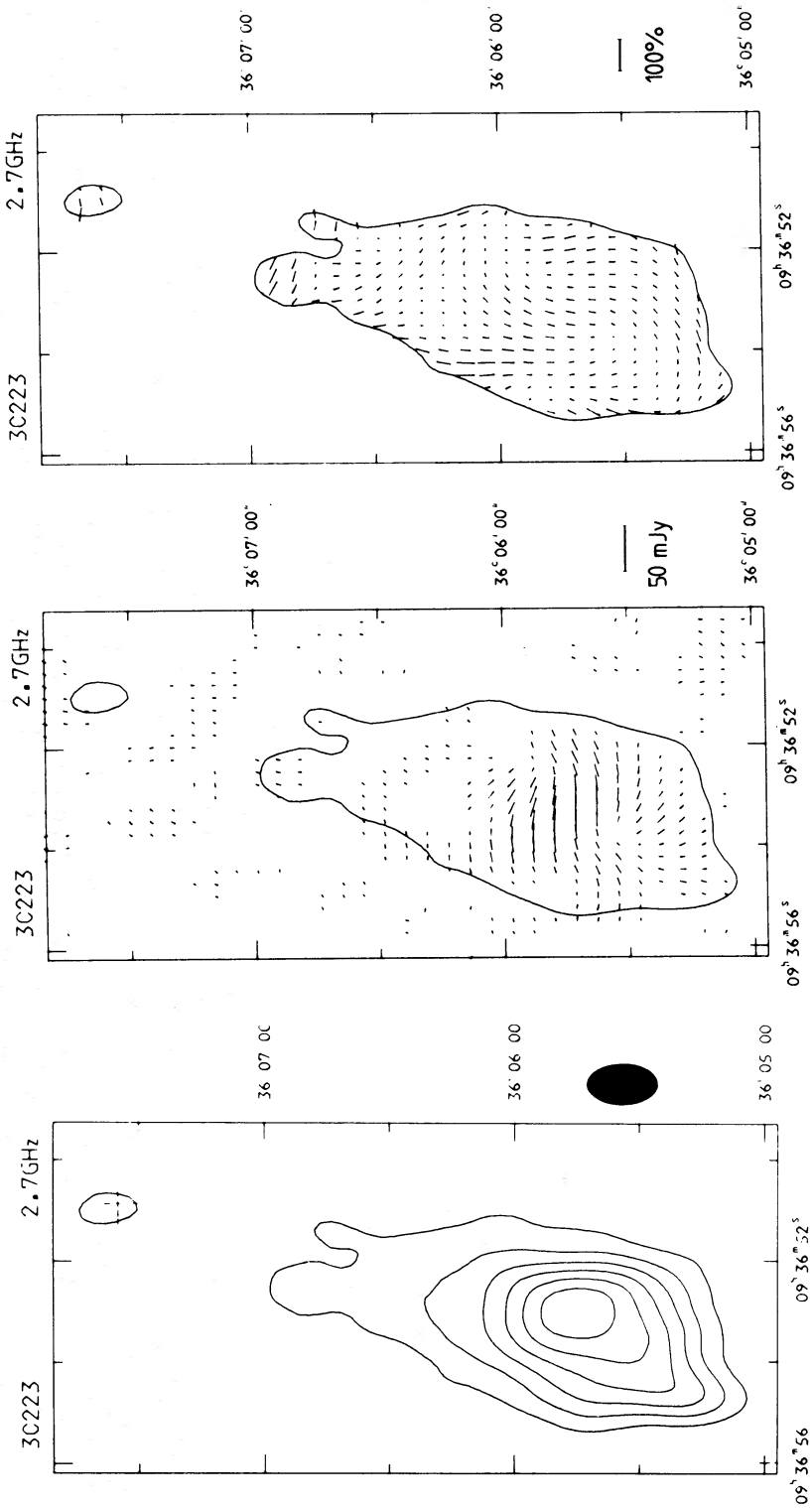

(d)

Figure 4 – *continued*

© Royal Astronomical Society • Provided by the NASA Astrophysics Data System

1985MNRAS.215..773M

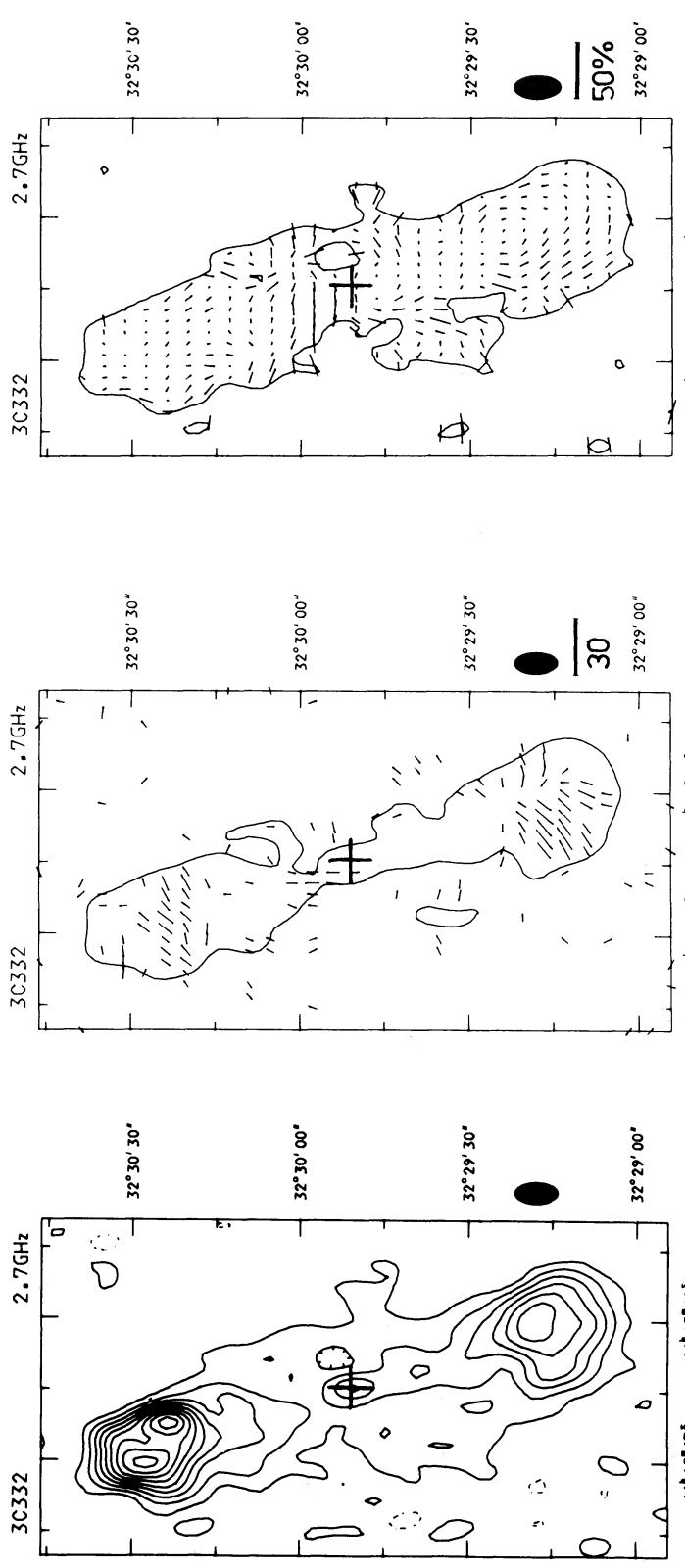

Figure 5. 3C 332 at 2.7 GHz. Captions as for Fig. 1, except as follows: (a) contour levels −4, 4, 12, 20, 28, 36, 44, 52, 60, 68 mJy beam^{-1} 7.09 K per mJy beam^{-1}; (b) vectors where $p<4$ mJy beam^{-1} are not shown; I contour at 10 mJy beam^{-1}; (c) vectors are not shown where $I<5$ mJy beam^{-1}; the correction for Faraday rotation is negligible.

© Royal Astronomical Society • Provided by the NASA Astrophysics Data System

1985MNRAS.215..773M

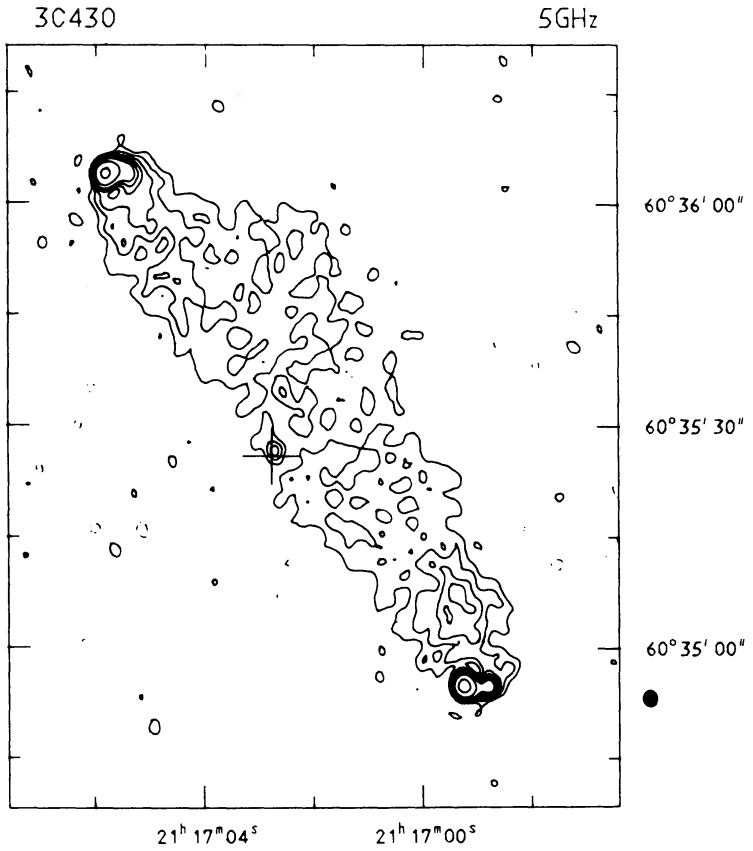

Figure 6. 3C 430 at 5 GHz. Map of total intensity, with contour levels at −5, 5, 10, 15, 20, 25, 30, 50, 100 mJy beam^{-1}. The scale of brightness temperature is 12.1 K per mJy beam^{-1}.

of relativistic electrons and magnetic fields, the pressure due to this plasma is 1/3 the energy density. Hence a minimum value for the lobe pressure may be evaluated from the value of the minimum energy density required to produce the observed emission. These values of minimum pressure can be used to show that most of the observed radio structures are probably not confined by external thermal gas pressure, on which limits can be placed from X-ray data (Miller *et al.*, 1985). In the present paper, the variation of pressure along the source is considered, and it is assumed that the variation in minimum pressure is related to the variation in actual pressure.

The minimum energy density (hereafter MED) was calculated from the standard formula, assuming no energy density in protons:

$$u=2.7\times10^{-16}\left\{\left[\frac{\nu_2^{1/2-\alpha}-\nu_1^{1/2-\alpha}}{1-2\alpha}\right]\nu_0^{2+\alpha}\frac{T}{D}(1+z)^{3+\alpha}\right\}^{4/7},$$

where ν_1 and ν_2 are the minimum and maximum frequencies observed in the observer's frame, T is the brightness temperature at an observed frequency ν_0, α is the spectral index between ν_1 and ν_2 (defined as $f_\nu \propto \nu^{-\alpha}$), z is the redshift of the source and D is the depth through the source, all in SI units. It was assumed that the radio spectra extend from 10 MHz to 15 GHz. The integrated source spectrum has been used in each case, with the flux density scale discussed by Laing & Peacock (1980). The magnetic field was assumed to be randomly oriented, and the depth through the source was estimated as the observed source width at the measured point perpendicular to the axis joining each hotspot with the central component. The depth through the source has a large uncertainty, but the resulting MED of a region with surface brightness S varies only as $(S/D)^{4/7}$. It

© Royal Astronomical Society • Provided by the NASA Astrophysics Data System

1985MNRAS.215..773M

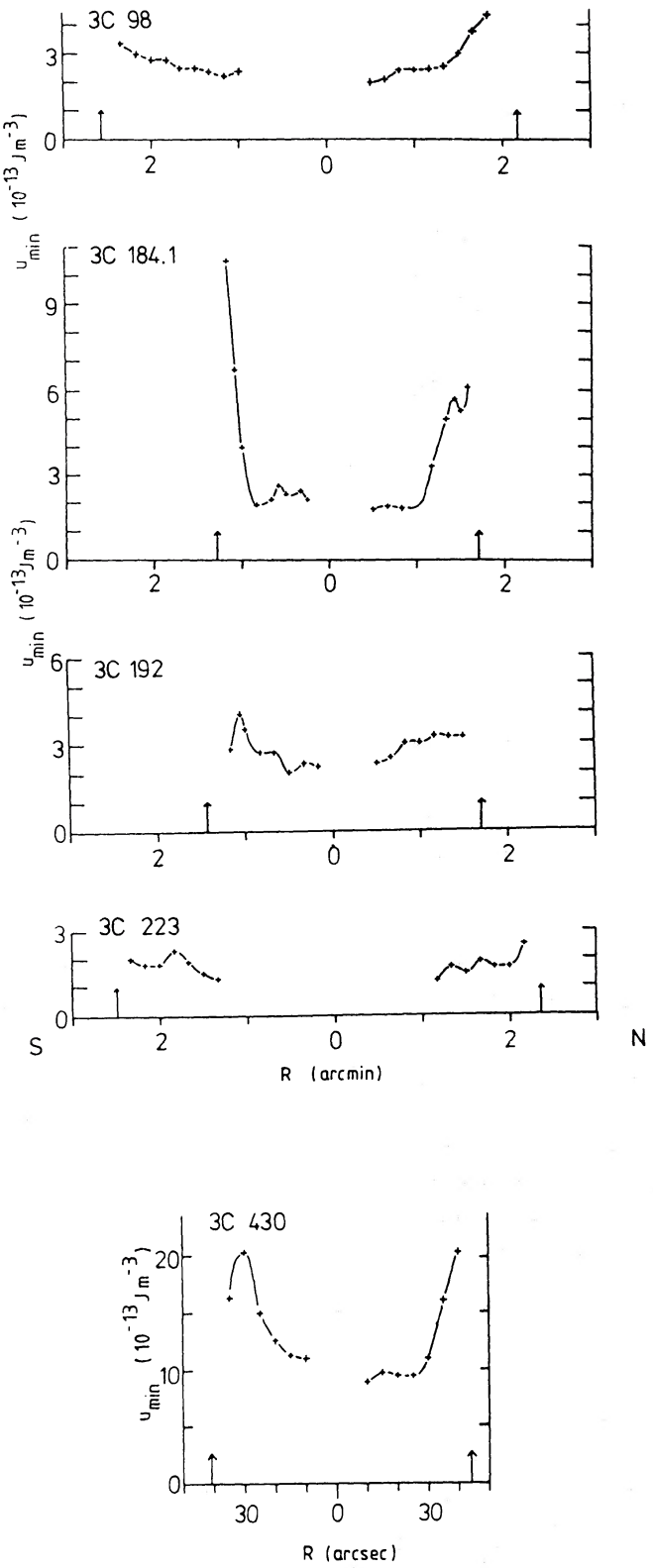

Figure 7. The distribution of minimum energy density (MED) along the major axes of five sources. The x-axis shows the angular distance away from the galaxy, and the y-axis shows the apparent minimum energy density in units of 10^{-13} J m^{-3}. The uncertainties in the MED are dominated by uncertainties in the 3-D structures and in the spectra of the lobes. Errors due to noise and zero-level uncertainties are generally smaller than the plotting symbols.

© Royal Astronomical Society • Provided by the NASA Astrophysics Data System

1985MNRAS.215..773M

can be seen from the radio maps that the assumed value of D does not greatly affect the overall variation in the MED, since the variation in surface brightness alone follows a similar distribution to the MED (see below). The distances to the source have been derived from the values of redshift given in Section 1, assuming values for Hubble's constant, H_0, of 50 km s^{-1} Mpc^{-1} and cosmological deceleration parameter, q_0, of 0.

There are some effects which increase the uncertainty in the MED:

(i) The observed source width is dependent on the surface brightness of the radio structure, and for regions of low brightness the width will be underestimated. This will be significant in regions with signal-to-noise ratios in the centre of the lobe less than about 3, and so the MED deduced in these regions is an overestimate.

(ii) Structures within the lobes will result in the MED lying between that in the larger-scale and smaller-scale structures. Such structures are visible close to the hotspots in 3C 98, 184.1 and 192, for example. Nevertheless, all the sources also have lobes with extensive areas of fairly constant surface brightness.

(iii) At the high frequencies used to map these sources, radiative losses could reduce the surface brightness in the lobe, without substantially altering the MED. Since the integrated spectra have been used, this could be important if spectral steepening occurs preferentially in one region. There is evidence of this in 3C 223, but not in 3C 192 (Högbom 1979). This is unlikely to affect the overall shape of the pressure distribution too severely, as lower-frequency maps still show lobes of constant surface brightness (Burch 1979a; Högbom & Carlsson 1974; Mackay 1969; Macdonald, Kenderdine & Neville 1968). Thus in some sources the MED could be underestimated by the assumption of an average spectral index, without seriously affecting the discussion.

The variation in MED along the source axes joining each hotspot with the central component is shown in Fig. 7 for five sources. The vertical arrows indicate the positions of the hotspots, which typically have lower limits on their MED which are a factor 10 higher than in the rest of the source. 3C 332 has been excluded as the estimates are completely dominated by the ridge structure. The errors in the MED are dominated by uncertainties in the 3-dimensional structure and in the electron energy spectrum, as discussed above. Errors due to the uncertainty in the zero-level or to noise are usually similar in magnitude to the size of the plotting symbols, except in the regions of lowest surface brightness. The MED was sampled at intervals of 10 and 5 arcsec (for the 2.7- and 5-GHz observations respectively) along the lobes, so that the plotted points are independent of each other. It is apparent from Fig. 7 that the derived minimum energy density in the sources appears fairly constant throughout the lobes, and rises in the brighter regions near the hotspots. The morphology of these regions is discussed below.

5 The morphology and magnetic field structure of the sources

The lobes in these sources appear to have two distinct regions. There is frequently a region extending 4–20 arcsec away from the hotspots, with a much higher MED than the rest of the lobe (Section 4) and a projected magnetic field structure parallel to the surface brightness contours. Such tails are observed in 3C 98 and 184.1, in 3C 219 (Burch 1979a, b), in 3C 381 (Laing 1981a; Miller & Laing, in preparation) and in many other sources (e.g. Laing 1981a; Jenkins *et al.* 1977). The relative contribution of the tails varies between sources – they are extremely prominent in 3C 184.1, but less so in 3C 98. Further in towards the galaxy the lobes have lower, more constant, MED, and tend to be broader. Hereafter, these regions will be referred to as bridges.

Various observers have noted that the projected magnetic field direction frequently lies parallel to the surface brightness contours (e.g. Högbom 1979; Laing 1981a). To explain such structure, Laing (1980, 1981b) has proposed a model in which the magnetic field has been

© Royal Astronomical Society • Provided by the NASA Astrophysics Data System

1985MNRAS.215..773M

compressed or sheared so as to be tangential to the source boundary (model C of Laing 1981b). The data presented here further reinforce the notion that dynamical effects associated with the large-scale structures of the sources are responsible for the observed magnetic field structures, since a mechanism is required which can produce both high fractional polarization and field directions which are directly correlated with the source morphology. The southern lobe of 3C 98 corresponds exactly to the predictions of model C for a lobe lying in the plane of the sky, since the fractional polarization is highest near the edges of the source and decreases to low values in the centre of the bridge, and the projected field direction is tangential to the source boundary. At other orientations of a lobe, the model predicts that the projected field is transverse in the central portion of the lobe and is surrounded by a tangential component.

In other sources where longitudinal fields are observed, however, the fractional polarization does not decrease to zero in the centre of the lobe as predicted. The lobes in 3C 223, the outer northern lobe of 3C 192 and 184.1, and the southern lobe of 3C 379.1 (Laing 1981a) have fractional polarizations of 25–50 per cent in their centres. In two sources with distorted lobes, 3C 192 and 20 (Laing 1981a), where the field directions lie parallel to the local axes of the lobes, the fractional polarizations are high in the centres of the distorted parts. These regions are all well resolved.

Högbom (1979) also noted fields perpendicular to source axes as described in Section 3. Examples are found in 3C 98, 184.1, 223, 349, 430 and 452 (Högbom 1979; Laing 1981a; Spangler *et al.* 1984; this paper). Laing's model predicts that regions of transverse field should occur over about half the width of the lobe, with the edges containing tangential fields. This does appear to be observed in the southern inner bridge of 3C 184.1, but there is no evidence for surrounding tangential fields in the other sources. Laing's model allows the field to be sheared perpendicular to the source axis close to the galaxy, because the contours of surface brightness often lie in that sense and the perpendicular component in 3C 452 could be explained thus. But whatever the description chosen, the physical mechanism by which such shearing arises is still unexplained.

Furthermore, in at least three sources, 3C 223, 349 (Laing 1981a) and 3C 452 (Högbom 1979), the field direction changes along the source axis, from longitudinal nearer the hotspots to transverse closer to the galaxy. This could arise in Laing's basic model if the lobe were distorted along the line-of-sight, but then it is surprising that no distortion is visible in the projected brightness distributions.

High fractional polarizations might be found in the centres of bridges if the surface brightness of the bridge were dominated by a jet structure, such as that possibly seen in 3C 332. In the other sources (i.e. 3C 98, 184.1, 192, and 223), however, the highly polarized regions are resolved, and they subtend a larger angle at the central component than do the hotspots. If the region is due to some particular structure in the bridge, then that structure is unlikely to be a jet.

Thus it seems that dynamical effects are important in shaping the magnetic field structures, and that in many cases Laing's model C can account for the observed configurations. Nevertheless, the physical mechanism by which this occurs is still unexplained, and further shearing, compression, or expansion seems to be required to provide a complete description of the observed structures.

6 A model for the FRII sources

6.1 THE CONTINUOUS-BEAM MODEL AND THE TANGENTIAL FIELD STRUCTURES

The model by Laing discussed above provides a satisfactory explanation of the magnetic field structures in many sources. In order to produce such large-scale structures from an initially tangled field by shearing or compression, work must have been done on the plasma, and a natural mechanism for this in the region of the hotspot is the conversion of bulk kinetic energy into

© Royal Astronomical Society • Provided by the NASA Astrophysics Data System

1985MNRAS.215..773M

internal energy. This can be achieved efficiently in a strong shock, for example, since a large part of the upstream kinetic energy is converted into internal energy. Field structures which have been compressed and sheared in this manner have a natural explanation in the continuous beam model (Blandford & Rees 1974, 1978; Scheuer 1974). In this model the hotspots are continuously supplied with energy, and possibly matter, by a beam from the central galaxy. Particles are accelerated in the hotspot, where they radiate, and therafter escape freely into the lobe. The beam entering the hotspot is thought to be supersonic, so that there is a shock at the end of the beam. The hotspot advances through the external medium at a speed governed by ram pressure balance, and it is thought that this advance speed is supersonic in the external medium so that a bow shock forms in front of the hotspot. The shocked beam and external media are separated by a contact discontinuity. Fermi acceleration in these shocks provides a possible mechanism for the acceleration of the relativistic particles (e.g. Drury 1983). Norman *et al.* (1982) and Wilson & Scheuer (1983) have presented numerical simulations of this model. Material passing from the beam and bow shocks would become compressed parallel to these shocks, and hence the magnetic field would tend to become compressed tangentially to the end boundary of the source (Blandford & Rees 1978). In addition, tangential shearing may occur in the plasma flow out of the hotspot. For many sources these processes are probably dominant, and result in the structures predicted by Laing's model.

6.2 THE FORMATION OF SHEARED FIELD STRUCTURES

In Section 5, however, evidence was presented for additional shearing and compression away from the hotspot, in the lobes of the sources. So far no physical explanation of how this might arise has been offered, but two simple considerations may provide some clues.

First, any non-relativistic plasma mixed in with the relativistic plasma would probably be hot, and hence fully ionized. Under these conditions, the magnetic field will be frozen-in to the plasma, owing to the high conductivity. The observed magnetic field structure then reflects the history of compression, stretching, and shearing to which the plasma has been subjected over its lifetime.

Secondly, there appears to be a pressure gradient between the hotspots and the rest of the bridge. The region of changing pressure is frequently resolved into regions which are referred to here as tails, although the pressure gradient could just as easily occur within an unresolved region, which would then simply be termed the hotspot.

The pressure gradient causes acceleration of the plasma in the opposite direction to the gradient, in a manner governed by Euler's equation. The flow is not steady, and the variation of flow velocity cannot be readily determined. Nevertheless, any given element of plasma must expand, because it ends up at a lower pressure, and the magnetic field will become stretched in the direction of expansion. If the plasma expands isotropically into the lobe the original field configuration will be preserved, but preferential expansion either longitudinally or laterally will produce appropriate large-scale configurations.

6.3 THE FLOW OF PLASMA

The pressure gradient causes the plasma to flow in the direction of the central galaxy when viewed from the plasma's initial rest frame, taken here to be the rest frame of the hotspot (since any residual flow of plasma after its injection through nearly-perpendicular beam or bow shocks should be subsonic). So, relative to the galaxy, the direction of the flow along the tail depends on whether the plasma experiences sufficient acceleration to overcome the initial velocity of the hotspot away from the galaxy. There is a maximum velocity attainable by the plasma relative to the hotspot which is about the initial sound speed, as can be seen from the equations of one-

© Royal Astronomical Society • Provided by the NASA Astrophysics Data System

1985MNRAS.215..773M

dimensional similarity flow (e.g. Landau & Lifshitz 1959). By integrating Euler's equation, using the adiabatic relation $P \propto \rho^{\gamma}$ and the equation of continuity, it may be shown that the maximum flow velocity, v_m, away from a region which is being maintained at a constant pressure with sound speed c_0, is given by

$$v_m = \frac{\gamma+1}{\gamma-1}\, c_0.$$

This velocity occurs at the boundary of flow into an initial vacuum, where the position of the boundary at time t after the start of the flow is $v_m t$. For regions much smaller than $c_0 t$, the flow is approximately steady-state, and the speed of the flow immediately out of the region of constant pressure is c_0.

The one-dimensional equations will not apply to the 3-dimensional flow in the region of the hotspot, but similar behaviour would be expected. If c_0 is much larger than the hotspot advance speed, v_H, then the flow out of the hotspot will be approximately steady-state, since the distance that sound can travel in the age of the source is much greater than the size of the hotspot. It is not obvious from these simple arguments what the flow out of the hotspot will be, since, in order to maintain steady-state flow along diverging streamlines from high to low pressure, the flow must be supersonic. The numerical simulations by Norman *et al.* (1982) suggest how such a flow may be achieved: in their simulation the flow initially travels along non-diverging streamlines, resulting in a low-pressure torus forming around the beam shock.

Hence, if the advance speed of the hotspot is greater than $v_m \sim c_0$, the plasma must flow away from the central galaxy in the latter's frame. The plasma expands along the source axis, the magnetic field lines become steadily more stretched longitudinally, and the surface brightness continually decreases. If, however, the advance velocity of the hotspot is sufficiently low, the plasma could flow towards the galaxy. The backflow of plasma could not continue indefinitely – eventually the plasma would run into material closer to the galaxy, and the pressure gradient would then flatten. This region would see an influx of matter which would compress the plasma in the lobe along the major axis. The magnetic field would become transverse to the source in this region, which would have a relatively high surface brightness and be visible as a bridge. High fractional polarization would be expected because, on average, source axes lie close to the plane of the sky so that random field components in the plane perpendicular to the source major axis do not reduce the fractional polarization (*cf.* Laing 1980).

In addition to the longitudinal flow and expansion, the plasma probably expands laterally into the external medium, since the tail regions do not appear to be statically confined by the thermal gas pressure of any external medium (Miller *et al.* 1985). If the internal density of thermal matter is lower than the external density, the lateral expansion into the external medium is governed by ram pressure balance, with the expansion speed lower than the internal sound speed of the plasma. If the contrast between external and internal densities is sufficiently large, then in regions of large pressure gradients the lateral expansion can be neglected compared with the longitudinal expansion, since the time-scale for the latter is determined by the initial internal sound speed.

At present, the ratio of densities is not determined observationally, although the continuous beam model allows some limits to be placed. Since the lobe cannot entrain more material than it sweeps away, the lobe density cannot be greater than the external density. The matter flux down the beam can be neglected, since the equations of ram pressure balance require that the matter flux density down the beam be no greater than the flux density of external matter through the hotspot, and so the flux of external matter entering the lobe must be larger than the flux of beam material entering the lobe. Since it is difficult for the external matter to become mixed with that in the lobe, except at the hotspot, the lobe density will probably be much less than the external density, as required for the longitudinal flow to dominate.

© Royal Astronomical Society • Provided by the NASA Astrophysics Data System

1985MNRAS.215..773M

6.4 THE INTERNAL SOUND SPEED

The ratio of the speed of advance of a hotspot to the sound speed in the hotspot, v_H/c_0, is a critical parameter, as it could determine whether a longitudinal or a transverse magnetic field is formed in the bridge. The instantaneous advance speed is given by $v_H \sim [P_H/\varrho_G)^{1/2}$, where P_H is the hotspot pressure and ϱ_G is the external density, while the sound speed $c_0 \sim (P_H/\varrho_H)^{1/2}$, where ϱ_H is the internal density.

Thus

$$\frac{v_H}{c_0} \sim \left(\frac{\varrho_H}{\varrho_G}\right)^{1/2}.$$

The time-averaged speed of advance could be significantly less than the instantaneous value, if the supplying beam moves laterally (Scheuer 1982). There is no evidence of this in these sources, but the possibility cannot be eliminated. The effect would be to increase the rate of backflow into the lobe.

In the numerical simulations by Norman *et al.* (1982), no mixing is allowed between the material passing through the beam and bow shocks, and it is the shocked beam material which forms the bridge. If the beam shock has an upstream Mach number M (>1), and if the plasma behaves as a perfect gas, the downstream, or hotspot, density is

$$\varrho_H = \frac{(\gamma+1)\,M^2}{(\gamma-1)\,M^2+2} \times \varrho_{beam}$$

(Landau & Lifshitz 1959), and hence

$$\frac{v_H}{c_0} \sim \left\{\frac{(\gamma+1)}{(\gamma-1)}\,\frac{\varrho_{beam}}{\varrho_G}\right\}^{1/2}.$$

This ratio is $\ll 1$ if $\varrho_{beam}/\varrho_G \ll 1$, and under these conditions significant backflow could occur. The dependence of the condition for backflow on M is small compared with that found numerically by Norman *et al.* The reason is that the backflow velocity can only become comparable with c_0 if the lobe pressure is much smaller than P_H. This is not the case in the simulations for low M by Norman *et al.* since the beam and lobe are in pressure equilibrium. But, if the lobe does not confine the beam, even beams with low M could generate substantial backflow.

If mixing between the shocked external and beam gases takes place, then ϱ_H is determined by the flow through the bow shock, since the matter flux density through the bow shock is larger than that through the beam shock by a factor $(\varrho_G/\varrho_{beam})^{1/2}$. For a strong bow shock,

$$\varrho_H \sim \frac{\gamma+1}{\gamma-1} \times \varrho_G$$

so

$$\frac{v_H}{c_0} \sim \left(\frac{\gamma+1}{\gamma-1}\right)^{1/2}$$

In this case there will be little backflow with respect to the galaxy, as in the case of high beam density above. Such mixing may be important owing to instabilities in the contact discontinuity near the hotspot (Norman *et al.* 1982).

Thus the variation in the ratio of advance speed to sound speed for a hotspot, the ratio of internal to external density, and the ratio of lobe pressure to hotspot pressure, all affect the net compression or expansion of the plasma. The variation of these quantities between sources may determine the dominant type of field structure observed – either longitudinal, transverse, or

© Royal Astronomical Society • Provided by the NASA Astrophysics Data System

1985MNRAS.215..773M

tangential – and may determine the surface brightness profile of the bridge. The variation of these parameters with time and with distance from the galaxy may account for the changes in the field direction observed.

7 Conclusions

Maps with 2- or 4-arcsec resolution have been presented for a number of double radio galaxies. The morphologies and projected magnetic field structures have been determined for most of them. At this resolution, high fractional polarizations, often in excess of 50 per cent, are observed, indicating well-ordered field structures when seen in projection. The projected field directions are extremely well correlated with the large-scale source structure, and are best explained by dynamical effects within the radio lobes (as in Laing 1981b).

Many of these sources have high-pressure regions extending up to 10 arcsec from each hotspot. These tails appear to have either tangential or longitudinal projected magnetic field directions. In sources with prominent bridges, the minimum pressure appears fairly constant outside the tail regions, and magnetic field directions are found to be either tangential to the source boundary, perpendicular to the source axis, or parallel to the source axis.

These field configurations can be qualitatively reproduced by a model which takes into account the flow of plasma into the lobe, and this history of compression, expansion and shearing of the plasma over its lifetime. In particular, the tangential configuration of Laing's (1980 & 1981b) model, and the longitudinal and transverse components of magnetic field described here may be direct results of the compression and shearing of plasma in the hotspot, followed by expansion along the tail into the low-pressure bridge. This simple scheme is consistent with the observations, and the resulting structures depend on a few basic parameters such as the ratio of hotspot advance speed to internal sound speed, the ratio of internal to external gas densities, and the relative pressures of the lobes and hotspots. In the continuous-beam models, the ratio of advance speed to sound speed is determined by the density contrast between beam and external medium, by the amount of mixing at the hotspot, and by the steadiness of the beam. For sources where the ratio is large, the plasma cannot flow backwards into the lobe, but continually expands behind the advancing hotspot. This expansion should be mainly along the source axis, resulting in longitudinal field directions. For lower values of the advance speed to sound speed, the plasma can fill the whole lobe, resulting in a bridge of constant pressure with a transverse magnetic field. The model predicts that transverse fields are seen in regions with low pressure gradients, whereas in regions with high pressure gradients the field structures should be either longitudinal or tangential (if only isotropic expansion occurs outside the hotspot). These predictions are in agreement with the observations presented here, and can be tested for other sources by observing the polarization of the extended radio structure with moderate resolution and high sensitivity.

Acknowledgments

I thank G. Pooley for his help with the observations, R. Saunders, P. Alexander and D. Green for mapping 3C 98, M. Brown for his help with earlier observations of 3C 98, and R. Saunders, J. Shakeshaft and P. Scheuer for their helpful comments. I also acknowledge financial support from an SERC studentship and the Cavendish Laboratory, and from an SERC postdoctoral fellowship during the completion of this work.

References

Blandford, R. D. & Rees, M. J., 1974. *Mon. Not. R. astr. Soc.*, **169**, 395.
Blandford, R. D. & Rees, M. J., 1978. *Phys. Scripta*, **17**, 265.

© Royal Astronomical Society • Provided by the NASA Astrophysics Data System

1985MNRAS.215..773M

Burch, S. F., 1979a. *Mon. Not. R. astr. Soc.,* **186,** 293.
Burch, S. F., 1979b. *Mon. Not. R. astr. Soc.,* **186,** 519.
Conway, R. G., Birch, P., Davis, R. J., Jones, L. R., Kerr, A. J. & Stannard, D., 1983. *Mon. Not. R. astr. Soc.,* **202,** 813.
Drury, L. O'C., 1983. *Rep. Prog. Phys.,* **46,** 973.
Fanaroff, B. L. & Riley, J. M., 1974. *Mon. Not. R. astr. Soc.,* **167,** 31P.
Haves, P., 1975. *Mon. Not. R. astr. Soc.,* **173,** 553.
Högbom, J. A., 1979. *Astr. Astrophys. Suppl.,* **36,** 173.
Högbom, J. A. & Carlsson, I., 1974. *Astr. Astrophys.,* **34,** 341.
Jenkins, C. J., Pooley, G. G. & Riley, J. M., 1977. *Mem. R. astr. Soc.,* **84,** 61.
Laing, R. A., 1980 *Mon. Not. R. astr. Soc.,* **193,** 439.
Laing, R. A., 1981a. *Mon. Not. R. astr. Soc.,* **195,** 261.
Laing, R. A., 1981b. *Astrophys. J.,* **248,** 87.
Laing, R. A. & Peacock, J. A., 1980. *Mon. Not. R. astr. Soc.,* **190,** 903.
Laing, R. A., Riley, J. M. & Longair, M. S., 1983. *Mon. Not. R. astr. Soc.,* **204,** 151.
Landau, L. D. & Lifshitz, E. M., 1959. *Fluid Mechanics,* Pergamon Press, Oxford.
Macdonald, G. H., Kenderdine, S. & Neville, A. C., 1968. *Mon. Not. R. astr. Soc.,* **138,** 259.
Mackay, C. D., 1969. *Mon. Not. R. astr. Soc.,* **145,** 31.
Miller, L., Longair, M. S., Fabbiano, G., Trinchieri, G. & Elvis, M., 1985. *Mon. Not. R. astr. Soc.,*
Norman, M. L., Smarr, L., Winkler, K.-H. A. & Smith, M. D., 1982. *Astr. Astrophys.,* **113,** 285.
Riley, J. M. & Pooley, G. G., 1975. *Mem. R. astr. Soc.,* **80,** 105.
Ryle, M., 1972. *Nature,* **194,** 517.
Scheuer, P. A. G., 1974. *Mon. Not. R. astr. Soc.,* **166,** 513.
Scheuer, P. A. G., 1982. *IAU Symp. No. 97,* pp. 163, eds Heeschen, D. S. & Wade, C. M., Reidel, Dordrecht, Holland.
Smith, H. E. & Spinrad, H., 1980. *Publs astr. Soc. Pacif.,* **92,** 553.
Spangler, S. R., Myers, S. T. & Pogge, J. J., 1984. *Astr. J.,* **89,** 1478.
Wilson, M. J. & Scheuer, P. A. G., 1983. *Mon. Not. R. astr. Soc.,* **205,** 449.

© Royal Astronomical Society • Provided by the NASA Astrophysics Data System